ELSEVIER

Contents lists available at ScienceDirect

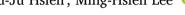
Computational Condensed Matter

journal homepage: www.elsevier.com/locate/cocom



A new strategy of getting accurate refractive index dispersion curves using first-principles sum-over-states method jointed by density functional perturbation theory

Yu-Ju Hsieh, Ming-Hsien Lee * 0



Department of Physics, Tamkang University, New Taipei City, 25137, Taiwan

ARTICLE INFO

Keywords: Refractive indices Sum-over-states Density-functional perturbation theory Nonlinear optical compounds

ABSTRACT

This paper introduces a new method for obtaining refractive index dispersion curves: the joint method of density-functional perturbation theory and first-principles sum-over-states. Since the refractive index dispersion curves and birefringence of LiNbO₃, LiGaSe₂ and BPO₄ materials computed by the first-principles sum-over-states method have some deviations, the density-functional perturbation theory method is introduced. However, the density-functional perturbation theory method can only obtain the refractive index at the optical frequency, so the first-principles sum-over-states combined with the density-functional perturbation theory method can be used to obtain the accurate refractive index dispersion curve. To further investigate the effect of parameters on the refractive index and birefringence, the different functionals, different cutoff energies, different *k*-points, ionic contributions and fixed symmetry are introduced for LiNbO₃, LiGaSe₂ and BPO₄ materials. The results show that symmetry-fixed nature of sum-over-states method is an important factor affecting the accuracy of the calculated birefringence.

1. Introduction

During the past decades, nonlinear optical (NLO) materials and birefringent materials have attracted much attention due to their unique properties and potential applications, such as electro-optical phase modulation, parametric oscillations, polarization-controlled devices, and holographic storage [1-5], among others. Many nonlinear optical compounds and birefringent materials have been designed and synthesized, examples like KBe₂BO₃F₂ (KBBF) [6], KH₂PO₄ (KDP) [7], CsLiB₆O₁₀ (CLBO) [8], KTiOPO₄ (KTP) [9], LiB₃O₅ (LBO) [10], β-BaB₂O₄ (BBO) [11], $Rb_2ScB_3O_6F_2$ [12], $Ca_2B_3O_6X$ (X = Cl and Br) [13], $Ba_3P_3O_{10}X$ (X = Cl, Br) [14], $A_3PbBi(P_2O_7)_2$ (A = Cs, Rb) [15], $CsPbCO_3F$ [16], Pb_2BO_3X (X = Cl, Br, I) [17], $AlBeBO_3F_2$ [18], MoX_2 (X = S, Se) [19], GaX (X = S, Se, Te) [20], GeC, [21], etc. In particular, KBBF is the only nonlinear optical material capable of output of deep ultraviolet lasers through the sixth harmonic generation. However, these crystals also have limitations. For example, KBBF poses significant challenges, including problems with layered growth habits, which makes it difficult to fabricate large crystals; the presence of toxic beryllium in the crystals, which raises environmental and health concerns. These limitations underscore the need for continuing research and development to discover and optimize next-generation NLO compounds and birefringent materials.

To advance the development of excellent nonlinear compounds, the implementation of computation-assisted strategies is essential [22–30]. Currently, several computational methodologies are employed in the field of nonlinear optics: (1) Empirical and Semi-Empirical Models: These models are utilized to explore and design compounds with optimal structural characteristics [31,32]. By leveraging established relationships between molecular structure and optical properties, researchers can efficiently identify candidates that exhibit favorable nonlinear optical behaviors. (2) First-Principles Methods: The first-principles methods, usually density functional theory (DFT), play a crucial role in evaluating the electronic properties of materials [33]. DFT is employed to calculate key parameters such as band gap, birefringence, and second harmonic generation (SHG) coefficients. These calculations provide insights into the viability of selected compounds, enabling the identification of materials with the potential for enhanced nonlinear optical performance. (3) Recently developed Machine Learning Approaches: Machine learning techniques are increasingly being integrated into the computational workflow to predict the structural and optical properties of materials. By fitting machine learning potentials to existing

E-mail address: mhslee@mail.tku.edu.tw (M.-H. Lee).

^{*} Corresponding author.

data, these approaches can accurately estimate the band gap, birefringence, and SHG coefficients of novel compounds. This predictive capability accelerates the discovery process by allowing for rapid screening of potential candidates based on their predicted performance.

It is well known that an excellent nonlinear optical compounds should meet a series of stringent requirements [34]: (1) Non-centrosymmetric (NCS) structures, (2) High transparency across the working spectral region, (3) Large second harmonic generation (SHG) coefficients (χ^2), (4) Appropriate birefringence (Δ n) to meet the phase-matching conditions, (5) High laser-induced damage threshold (LIDT), and (6) Good physicochemical stability and feasibility of large crystal growth. Hence how to get accurate refractive indices and birefringence play an important role in understanding structure-property relationship and discovering novel nonlinear optical compounds. First-principles sum-over-states (SOS) method is commonly applied to calculate the refractive index and birefringence of materials. However, there are discrepancies between the refractive indices and birefringence calculated using the first-principles SOS method and the experimental values. For example, for ultraviolet and deep-ultraviolet materials, the underestimation of the band gap due to the approximation of density-functional theory using exchange-correlation functional results in refractive index predictions that deviate from experimental data. For infrared materials, the computational and experimental results were found to be significantly different due to the lack of phonon effects in the first-principles optical property calculations [35].

To obtain more accurate computational data, density-functional perturbation theory (DFPT) was introduced. As described in the online manul of CASTEP, the DFPT or so-called linear response theory provides a way of computing the second derivative of the total energy with respect to a given perturbation [36]. And if the perturbation is an electric field, it can be used to calculate the dielectric response and so on, and then it can be used to calculate the refractive indices and birefringence. Lots of literature has reported the Born effective charge tensors, dielectric constants and so on calculated by the density-functional perturbation theory [37–40]. And scientists have also tried to investigate the optical properties using multiple strategies. For example, Hu et al. have investigated the THz absorption by applying density function perturbation theory plus the Lorentzian line [41].

In this study, the refractive index and birefringence of classical materials are calculated using both DFPT and first-principle SOS methods, respectively. It is found that the refractive indices of birefringence of LiNbO₃, LiGaSe₂ and BPO₄ materials obtained by first principle sumover-states method do not agree with the experimental values. Interestingly, the birefringence of LiNbO3, LiGaSe2 and BPO4 materials obtained by DFPT agrees with the experimental values. Unfortunately, density-functional perturbation theory can only obtain the permittivity of the optical frequency, and then it can only get the refractive index and birefringence at a special wavelength. We therefore propose a new strategy for obtaining refractive index dispersion curves: the joint method of DFPT and first-principles SOS. The refractive index dispersion curves obtained by the joint method of DFPT and first-principle SOS are in good agreement with the experiment. In order to investigate the influencing factors affecting the calculation of refractive index and birefringence, different plane wave cutoff energies, different Monkhorst-Pack k-point meshes in the Brillouin zones, different functionals (the GGA with PBE and local-density approximation (LDA) functionals), ionic contributions and fixed symmetry are introduced for LiNbO₃, LiGaSe2 and BPO4 materials.

2. Calculation details

2.1. General parameters

In this paper, the geometries relaxation and electronic structures were firstly calculated using the density functional method implemented in CASTEP code [42]. The crystallographic information files (CIF) of

compounds were obtained from the inorganic crystal structure database (ICSD, Version 5.2.0) [43], such as BPO₄ (ICSD-55082), LiNbO₃ (ICSD-61118) and LiGaSe2 (ICSD-146955). During the calculation, the generalized gradient approximation (GGA) [44] Perdew-Burke-Ernzerhof (PBE) [45] functional and norm-conserving pseudopotential (NCP) [46] were adopted. To achieve convergence in geometry optimization, the total energy convergence criterion was set to 5.0×10^{-6} eV, while the convergence criteria for maximum atomic force, maximum stress, and maximum displacement were set to 0.01 eV/Å, 0.02 GPa, and 5.0×10^{-4} Å, respectively.

2.2. Details about SOS method

Based on the obtained electronic structures, the dielectric function $\varepsilon(\omega)=\epsilon_{\infty}^{(1)}(\omega)+\mathrm{i}\epsilon_{\infty}^{(2)}(\omega)$ can be obtained using the so-called sum-overstates (SOS) method. Under SOS method, the imaginary part of the dielectric function is expressed as follows:

$$\epsilon_{\infty}^{(2)}(\omega) = 2\frac{4\pi^2}{\Omega}\frac{1}{\Omega^2}\frac{1}{N_{\rm k}}\sum_{n\,m\,k}(f_{n{\rm k}}-f_{m{\rm k}})|\lambda\cdot p_{nm}|^2\delta(\varepsilon_{m{\rm k}}-\varepsilon_{n{\rm k}}-\hbar\omega)$$

where ω is the angular frequency of the photon, Ω is the volume of the unit cell, N_k is the integration measure in momentum space, $f_{nk}-f_{mk}$ is the difference between the occupation numbers of electrons at band n and momentum k and band m and momentum k, ε_{nk} is the energy eigenstate of the electron, p_{nm} is the momentum matrix element between bands n and m, and λ is the coupling strength of the light field.

The real part is obtained through Kramers–Kronig transformation as follows [47]:

$$\epsilon_{\infty}^{(1)}(\omega) = 1 + \frac{1}{\pi} \int_{0}^{\infty} \frac{\epsilon_{\infty}^{(2)}(\omega')\omega'}{\omega'^2 - \omega^2} d\omega'$$

The refractive index $n(\omega)$ is expressed as follows:

$$n(\omega) = \left[\frac{\sqrt{\epsilon_1^2 + \epsilon_2^2} + \epsilon_1^2}{2} \right]^{\frac{1}{2}}$$

2.3. Details about DFPT method

To obtain more accurate computational data, density-functional perturbation theory (DFPT) was introduced. DFPT obtains the charge density and polarization response by solving the wavefunction corrections under perturbation, which leads to the permittivity of the optical frequency, and ultimately the refractive index and birefringence. Thus the expression for the permittivity is [48]:

$$\varepsilon_{total} = \varepsilon_{\infty} + \sum_{u} \varepsilon_{u}$$

Where ε_{∞} is the electronic contribution and ε_u is the oscillator strength for mode u. The ionic contribution is included by perturbing the structure along certain directions and calculating the resulting polarization.

$$\varepsilon_{u} = \sum_{\alpha\beta ij_{k}} \frac{z_{\alpha,ij}^{*} z_{\beta,i}^{*} a_{u,\alpha j} a_{u,\beta j}}{\frac{1}{3m_{\alpha}^{2}} 3m_{\beta}^{\frac{1}{2}} \Omega \varepsilon_{0} \omega_{u}^{2}}$$

where $\mathbf{z}_{a,i}^*$ is the Born effective charge of ion α , Ω is the supercell volume, m_α is the mass of ion α , ε_0 is the free-space dielectric constant and ω_u are the eigenmode.

2.4. Other details

For further investigating the effect of parameters on refractive index and birefringence, the electronic structures and optical properties of LiNbO₃, LiGaSe₂ and BPO₄ materials were further calculated using

Table 1The birefringence and refractive indices of experimental and calculated by the DFPT and SOS method.

Compound	Space Group	n_{o}	$n_{\rm e}$	Δ n-Efield	n_{o}	$n_{\rm e}$	Δn -SOS	Experimental value
LiNbO ₃ LiGaSe ₂	R3c Pna2 ₁	2.476 2.356	2.410 2.408	-0.066 0.053	2.743 2.601	2.551 2.611	-0.192 0.010	-0.074 0.051
BPO ₄	I 4	1.611	1.622	0.011	1.662	1.650	-0.012	0.005

different plane wave cutoff energies, different Monkhorst-Pack k-point meshes in the Brillouin zones [49],and different functionals (the GGA with PBE and local-density approximation (LDA) functionals shown in Table 2 and Table S1–S3 in SI [50].

3. Results and discussion

The refractive indices and birefringence of various materials have been calculated using the density-functional perturbation theory (DFPT) and first-principle sum-over-states (SOS) method, with results summarized in Table 1 and SI Table S3. Both methods usually provide birefringence values comparable to experimental results. For most materials the absolute errors are less than 30 % and 35 % for the densityfunctional perturbation theory and first-principles state summation methods, respectively; very little material has deviations from experimental values for both methods, such as the KAlSi₃O₈ material. However, discrepancies are observed for certain materials such as LiNbO₃, LiGaSe₂, and BPO₄ using first-principle SOS method. For instance, in the case of BPO₄, the ordinary refractive index (n_0) is calculated as 1.662, the extraordinary refractive index (n_e) as 1.650, and the birefringence $(\Delta n = n_e - n_o)$ as -0.012. This contrasts with the experimentally measured birefringence of 0.005. Similarly, for LiNbO3, the birefringence derived from the first-principle SOS method is -0.192, approximately three times the experimental value of -0.074. Conversely, for LiGaSe2, the calculated birefringence of 0.010 is only one-fifth of the experimental value. Interestingly, calculations using DFPT yield birefringence values more consistent with experimental results. Specifically, the birefringence values for LiNbO₃, LiGaSe₂, and BPO₄ are −0.066, 0.053, and 0.011, respectively, which closely match their corresponding experimental values of -0.074, 0.051, and 0.005 [51-53]. However, the DFPT can only provide birefringence at limiting frequency, it cannot generate the full refractive index dispersion curves of the materials because it only yields the permittivity at the long wavelength frequency.

To address this, a novel joint approach combining the first-principle SOS and DFPT has been proposed for deriving refractive index dispersion curves. The methodology is illustrated in Fig. 1 and involves several key steps. Firstly, the refractive indices and birefringence were obtained using both the SOS method and DFPT method. Noting that the SOS method can get refractive indices at very wide energy range from DUV to IR energy region (like the refractive indices curve shown in Fig. 2), while the DFPT method can only get refractive indices at optical frequency. Secondly, due to the DFPT method can get more reliable birefringence, hence the refractive indices dispersion curve obtained by SOS method is shifted until the refractive indices obtained by SOS at optical frequency is same as the one obtained by DFPT. And now, new refractive indices dispersion curves were obtained using the jointed strategy described above. As depicted in Fig. 2, the dashed lines represent the refractive index dispersion curves for ordinary and extraordinary light calculated using the first-principle SOS method. In contrast, the smooth solid lines correspond to the dispersion curves obtained via the joint approach. For comparison, the experimental dispersion curves for ordinary and extraordinary light are shown as solid lines with embedded data points. Fig. 2 highlights that the refractive index dispersion curves derived from the joint method exhibit agreement with the experimental results. This consistency highlights the precision and robustness of the joint approach, which seamlessly combines the point-specific refractive index calculations from DFPT with the comprehensive dispersion data provided by the sum-over-states method. As a result, the joint method offers a reliable and precise approach for modeling the optical dispersion characteristics of nonlinear optical materials.

The data indicate that the refractive indices and birefringence of $LiNbO_3$, $LiGaSe_2$, and BPO_4 calculated using density-functional perturbation theory (DFPT) align more closely with experimental values compared to those obtained from the first-principle sum-over-states method. Previous studies have explored factors influencing the accuracy of refractive index and birefringence calculations, including plane wave

Table 2
The birefringence corresponding to different cut-off energies, *k*-points, different functionals, with or without ionic contribution (i) are calculated for LiNbO₃, LiGaSe₂ and BPO₄ materials by DFPT.

compound	functional	Cut-off energy	k-point	Δ n-Efield	Δn -SOS	Expt. value
BPO ₄	GGA	830	14 × 14 × 16	0.011	-0.012	0.005
BPO ₄	GGA	830	$9 \times 9 \times 11$	0.011	-0.012	
BPO ₄	GGA	830	$7 \times 7 \times 8$	0.011	-0.012	
BPO ₄ (i)	GGA	830	$7 \times 7 \times 8$	0.011	-0.012	
BPO ₄	GGA	750	$7 \times 7 \times 8$	0.011	-0.012	
BPO ₄	GGA	600	$7 \times 7 \times 8$	0.012	-0.013	
BPO ₄	LDA	830	$7\times7\times8$	0.008	-0.012	
LiNbO ₃	GGA	750	$\overline{12 imes 12 imes 12}$	-0.097	-0.1928	-0.0738
LiNbO ₃	GGA	750	$8 \times 8 \times 8$	-0.097	-0.1928	
LiNbO ₃	GGA	750	$6 \times 6 \times 6$	-0.097	-0.1928	
LiNbO ₃ (i)	GGA	750	$6 \times 6 \times 6$	-0.097	-0.1928	
LiNbO ₃	GGA	830	$6 \times 6 \times 6$	-0.097	-0.1928	
LiNbO ₃	GGA	600	$6 \times 6 \times 6$	-0.095	-0.1923	
LiNbO ₃	LDA	750	$6 \times 6 \times 6$	-0.101	-0.1939	
LiGaSe ₂	GGA	880	$7 \times 6 \times 8$	0.058	0.005	0.0509
LiGaSe ₂	GGA	880	$5 \times 4 \times 5$	0.061	0.004	
LiGaSe ₂	GGA	880	$4 \times 3 \times 4$	0.042	0.005	
LiGaSe ₂ (i)	GGA	880	$4 \times 3 \times 4$	0.036	0.004	
LiGaSe ₂	GGA	800	$4 \times 3 \times 4$	0.042	0.006	
LiGaSe ₂	GGA	590	$4 \times 3 \times 4$	0.046	0.006	
$LiGaSe_2$	LDA	880	$4 \times 3 \times 4$	0.038	0.003	

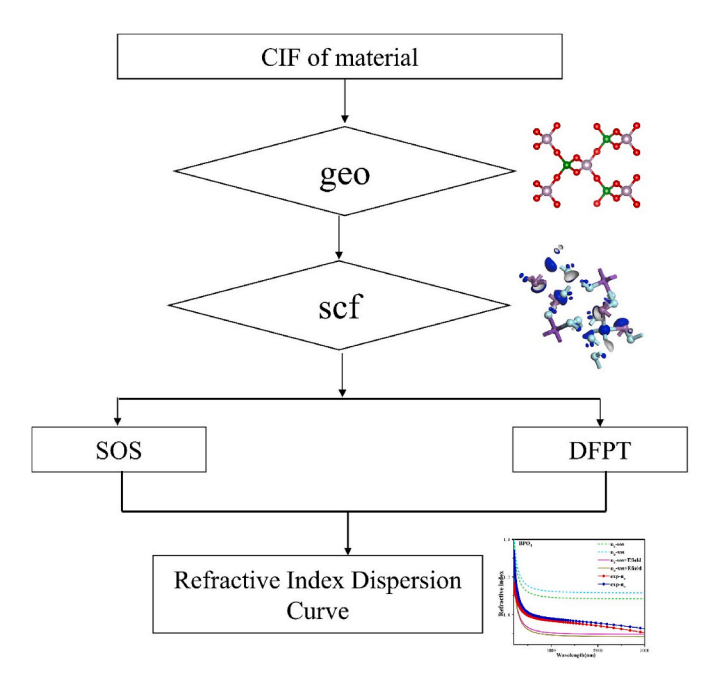


Fig. 1. Refractive index dispersion curves obtained by a joint method of the first-principle sum-over-states and density-functional perturbation theory.

cutoff energy, Monkhorst-Pack k-point meshes in the Brillouin zones, functionals (the GGA with PBE and local-density approximation (LDA) functionals) and ionic contributions. In order to investigate the influencing factors affecting the calculation of refractive index and

birefringence, different plane wave cutoff energies, different Monkhorst-Pack k-point meshes in the Brillouin zones, different functionals (the GGA with PBE and local-density approximation (LDA) functionals) and ionic contributions are introduced for LiNbO3, LiGaSe2 and BPO4 materials in Table 2. For BPO4, it was observed that increasing the plane wave cutoff energy from 600 eV to 830 eV using DFPT altered the refractive index and birefringence by only 0.001, while no changes were observed when using the first-principle SOS method. Similarly, with or without ionic contribution and increasing the k-point density did not affect the calculated refractive index and birefringence of BPO₄. When the applied functional was modified from GGA/PBE to LDA, the birefringence obtained by DFPT varied marginally from 0.008 to 0.011, while no changes were observed in the birefringence values calculated using the SOS method. These results suggest that the calculated refractive index and birefringence remain effectively invariant under changes in cutoff energy, k-point density, functionals, and ionic contributions for both DFPT and the sum-over-states method. In summary, the impact of variations in computational parameters, including cutoff energy, kpoints, functionals, and ionic contributions, on the refractive index and birefringence calculations is negligible.

To further explore the factors influencing refractive index and birefringence calculations using the density-functional perturbation theory (DFPT) method, fixed symmetry constraints were introduced by modifying the CASTEP code. The results, summarized in Table 3, reveal intriguing trends. Specifically, the birefringence values for BPO $_4$ and LiNbO $_3$ calculated using DFPT with fixed symmetry are -0.012 and -0.175, respectively, closely aligned with the birefringence values obtained through the first-principle sum-over-states method. However, when fixed symmetry is introduced, the birefringence of the LiGaSe $_2$ becomes nearly twice as much compared to the previous one without

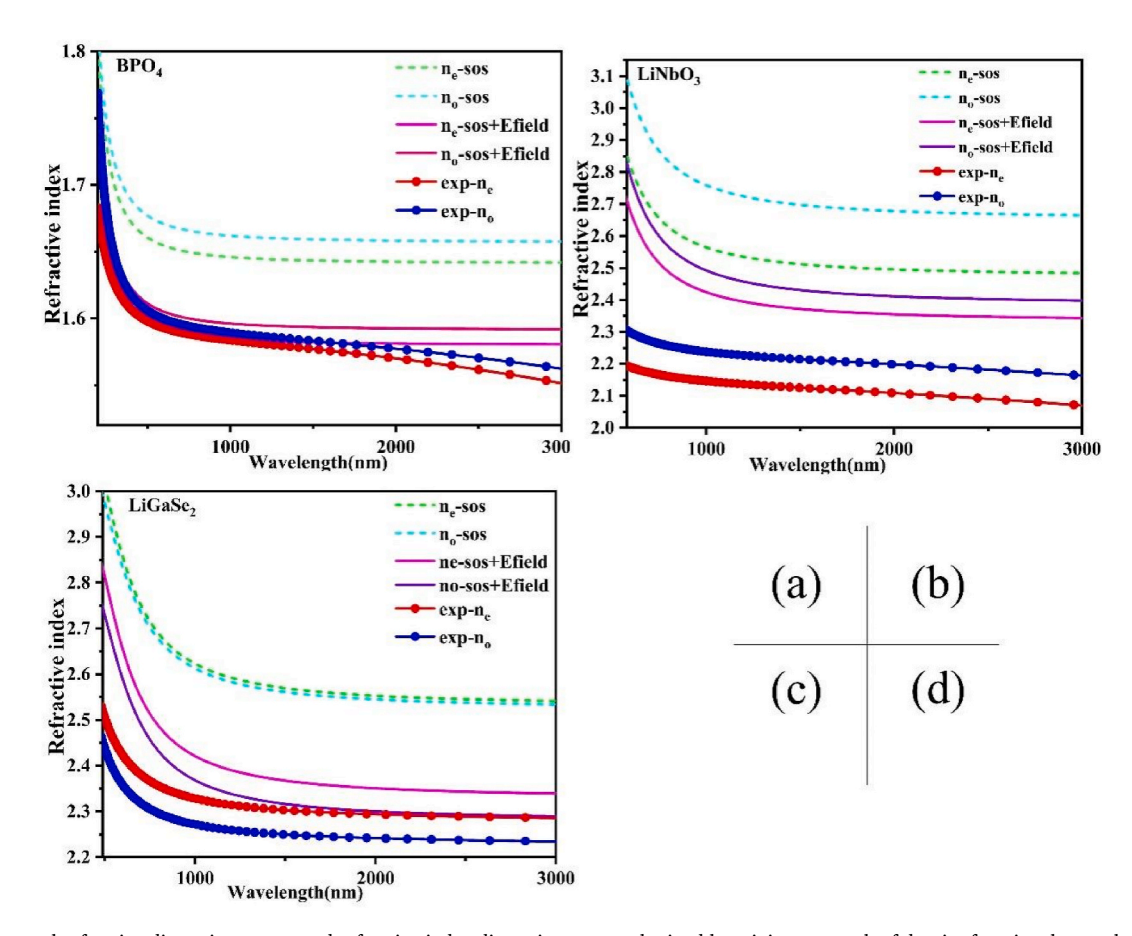


Fig. 2. Experimental refractive dispersion curves and refractive index dispersion curves obtained by a joint approach of density-functional perturbation theory and the first-principle sum-over-states methods.

Table 3The birefringence and refractive indices of fix symmetry by density-functional perturbation theory.

Compound	Space Group	n _e	n_{o}	Δ n-Fix symmetry	Δn -SOS	Experimental value
LiNbO ₃	R3c	2.391	2.566	-0.175	-0.192	-0.074
LiGaSe ₂	$Pna2_1$	2.498	2.390	0.108	0.010	0.051
BPO ₄	I 4	1.606	1.618	-0.012	-0.016	0.005

fixed symmetry by density-functional perturbation theory. These findings suggest that, at least for some crystals, the failure of SOS to reproduce experimental birefringence is simply because symmetry not treated broken during electronic (optical) excitation, while DFPT does it correctly. Comparisons for more crystals calculated with this symmetry-fixed DFPT are shown in Table S4 of SI.

4. Conclusions

In this paper, a new strategy jointed with the SOS refractive indices dispersion curve and DFPT refractive indices at optical frequency is proposed. The results show that the new jointed strategy can get not only more accurate results at optical frequency but also reliable refractive indices dispersion curve, which can be further used to predict and screen novel birefringent and nonlinear optical compounds. And this paper also discussed the factors like symmetry, cutoff energies and so on, which could lead errors to prediction of birefringence using the new strategy, and these discussions can help to get reliable results under the proposed strategy.

CRediT authorship contribution statement

Yu-Ju Hsieh: Writing – review & editing, Writing – original draft, Investigation. **Ming-Hsien Lee:** Supervision, Methodology.

Declaration of competing interest

The authors declare that they have no known competing financial interests or personal relationships that could have appeared to influence the work reported in this paper.

Acknowledgments

MHL would like to thank academician Prof. T-K. Lee for the useful discussion and comments in the early stage of this research. Authors wish to express their deepest gratitude for the enormous help from Prof. Qun Jing in Xinjiang University during the completion of the present work.

Appendix A. Supplementary data

Supplementary data to this article can be found online at https://doi.org/10.1016/j.cocom.2025.e01066.

Data availability

Data will be made available on request.

References

- [1] Y. Shi, S. Pan, X. Dong, Y. Wang, M. Zhang, F. Zhang, Z. Zhou, Na3Cd3B(PO4)4: A new noncentrosymmetric borophosphate with zero-dimensional anion units, Inorg. Chem. 51 (2012) 10870–10875.
- [2] T. Sasaki, Y. Mori, M. Yoshimura, Y.K. Yap, T. Kamimura, Recent development of nonlinear optical borate crystals: key materials for generation of visible and UV light, Mater. Sci. Eng. R Rep. 30 (2000) 1–54.
- [3] S. Pan, J.P. Smit, B. Watkins, M.R. Marvel, C.L. Stern, K.R. Poeppelmeier, Synthesis, crystal structure, and nonlinear optical properties of Li6CuB4O10: a congruently melting compound with isolated [CuB4O10]6- units, J. Am. Chem. Soc. 128 (2006) 11631–11634.

- [4] L. Wang, S. Pan, L. Chang, J. Hu, H. Yu, UV nonlinear optical crystal Ba2[B609 (OH)4] featuring unique chiral layers with a new B18O42 circle based on BO3 and BO4 units, Inorg. Chem. 51 (2012) 1852–1858.
- [5] H. Wu, S. Pan, K.R. Poeppelmeier, H. Li, D. Jia, Z. Chen, X. Fan, Y. Yang, J. M. Rondinelli, H. Luo, K3B6010Cl: a new structure analogous to perovskite with a large second harmonic generation response and deep UV absorption edge, J. Am. Chem. Soc. 133 (2011) 7786–7790.
- [6] B. Wu, D. Tang, N. Ye, C. Chen, Linear and nonlinear optical properties of the KBe2BO3F2 (KBBF) crystal, Opt. Mater. 5 (1996) 105–109.
- [7] Y.S. Liu, W.B. Jones, J.P. Chernoch, High-efficiency high-power coherent uv generation at 266 nm in 90° phase-matched deuterated KDP, Appl. Phys. Lett. 29 (1976) 32–34.
- [8] Y. Mori, I. Kuroda, S. Nakajima, T. Sasaki, S. Nakai, New nonlinear optical crystal: cesium lithium borate, Appl. Phys. Lett. 67 (1995) 1818–1820.
- [9] R.J. Bolt, M.H. van der Mooren, H. de Haas, Growth of KTiOPO4 (KTP) single crystals by means of phosphate and phosphate/sulfate fluxes out of a three-zone furnace, J. Cryst. Growth 114 (1991) 141–152.
- [10] C. Chen, Y. Wu, A. Jiang, B. Wu, G. You, R. Li, S. Lin, New nonlinear-optical crystal: LiB3O5, J. Opt. Soc. Am. B 6 (1989) 616–621.
- [11] D.N. Nikogosyan, Beta barium borate (BBO), Appl. Phys. A 52 (1991) 359-368.
- [12] Q. Zhang, R. An, X. Long, Z. Yang, S. Pan, Y. Yang, Exploiting deep-ultraviolet nonlinear optical material Rb2ScB3O6F2 originated from congruously oriented [B3O6] groups, Angew. Chem. Int. Ed. 64 (2025) e202415066.
- [13] H. Qiu, F. Li, Z. Li, Z. Yang, S. Pan, M. Mutailipu, Breaking the inherent interarrangement of [B306] clusters for nonlinear optics with orbital hybridization enhancement, J. Am. Chem. Soc. 145 (2023) 24401–24407.
- [14] P. Yu, L.-M. Wu, L.-J. Zhou, L. Chen, Deep-ultraviolet nonlinear optical crystals: $Ba3P3O10X\ (X=Cl, Br)$, J. Am. Chem. Soc. 136 (2014) 480–487.
- [15] X. Lu, Z. Chen, X. Shi, Q. Jing, M.-H. Lee, Two pyrophosphates with large birefringences and second-harmonic responses as ultraviolet nonlinear optical materials, Angew. Chem. Int. Ed. 59 (2020) 17648–17656.
- [16] G. Zou, L. Huang, N. Ye, C. Lin, W. Cheng, H. Huang, CsPbCO3F: A strong second-harmonic generation material derived from enhancement via p-π interaction, J. Am. Chem. Soc. 135 (2013) 18560–18566.
- [17] Y. Tang, X. Chen, M. Zhu, X. Liao, S. Hou, Y. Yu, X. Fan, The strong alternating built-in electric field sourced by ball milling on Pb2BO3X (XCl, Br, I) piezoelectric materials contributes to high catalytic activity, Nano Energy 101 (2022) 107545.
- [18] G. Yang, K. Wu, Designing two-dimensional KBBF family second-harmonic generation monolayers, J. Phys. Chem. C 122 (2018) 7992–7996.
- [19] C.-Y. Wang, G.-Y. Guo, Nonlinear optical properties of transition-metal dichalcogenide MX2 (M = Mo, W; X = S, Se) monolayers and trilayers from firstprinciples calculations, J. Phys. Chem. C 119 (2015) 13268–13276.
- [20] L. Hu, X. Huang, D. Wei, Layer-independent and layer-dependent nonlinear optical properties of two-dimensional GaX (X = S, Se, Te) nanosheets, Phys. Chem. Chem. Phys. 19 (2017) 11131–11141.
- [21] L. Hu, D. Wei, Second-order nonlinear optical properties of bulk GeC polytypes, g-GeC and corresponding nanotubes: first-principles calculations, Phys. Chem. Chem. Phys.: Phys. Chem. Chem. Phys. 19 (2017) 2235–2244.
- [22] Z.S. Lin, L. Kang, T. Zheng, R. He, H. Huang, C.T. Chen, Strategy for the optical property studies in ultraviolet nonlinear optical crystals from density functional theory, Comput. Mater. Sci. 60 (2012) 99–104.
- [23] C. Chen, N. Ye, J. Lin, J. Jiang, W. Zeng, B. Wu, Computer-assisted search for nonlinear optical crystals, Adv. Mater. 11 (1999) 1071–1078.
- [24] B. Agrahari, S. Layek, R. Ganguly, N. Dege, D.D. Pathak, Synthesis, characterization and single crystal X-ray studies of pincer type Ni(II)-Schiff base complexes: application in synthesis of 2-substituted benzimidazoles, J. Organomet. Chem. 890 (2019) 13–20.
- [25] M.A. Raza, U. Farwa, M. Danish, S. Ozturk, A.A. Aagar, N. Dege, S.U. Rehman, A. G. Al-Sehemi, Computational modeling of imines based anti-oxidant and anti-esterases compounds: synthesis, single crystal and In-vitro assessment, Comput. Biol. Chem. 104 (2023) 107880.
- [26] S. Kansız, M. Azam, T. Basılı, S. Meral, F.A. Aktaş, S. Yeşilbağ, K. Min, A.A. Ağar, N. Dege, Synthesis, structural studies, Hirshfeld surface analysis, and molecular docking studies of a thiophene-based Schiff base compound, J. Mol. Struct. 1265 (2022) 133477
- [27] N. Arumugam, A.I. Almansour, R.S. Kumar, A.J. Mohammad Ali Al-Aizari, S. I. Alaqeel, S. Kansız, V.S. Krishna, D. Sriram, N. Dege, Regio- and diastereoselective synthesis of spiropyrroloquinoxaline grafted indole heterocyclic hybrids and evaluation of their anti-Mycobacterium tuberculosis activity, RSC Adv. 10 (2020) 23522–23531.
- [28] N. Dege, Ö. Özge, D. Avcı, A. Başoğlu, F. Sönmez, M. Yaman, Ö. Tamer, Y. Atalay, B. Zengin Kurt, Concentration effects on optical properties, DFT, crystal characterization and α-glucosidase activity studies: novel Zn(II) complex, Spectrochim. Acta Mol. Biomol. Spectrosc. 262 (2021) 120072.
- [29] S. Daoui, C. Baydere, F. Akman, F.E. Kalai, L. Mahi, N. Dege, Y. Topcu, K. Karrouchi, N. Benchat, Synthesis, X-ray crystallography, vibrational

- spectroscopy, thermal and DFT studies of (E)-6-(4-methylstyryl)-4,5-dihydropyridazin-3(2H)-one, J. Mol. Struct. 1225 (2021) 129180.
- [30] M.N. Tahir, M. Ashfaq, M. Feizi-Dehnayebi, K.S. Munawar, Ş. Atalay, N. Dege, N. Guliyeva, A. Sultan, Crystal structure, Hirshfeld surface analysis, computational study and molecular docking simulation of 4-aminoantipyrine derivative, J. Mol. Struct. 1320 (2025) 139747.
- [31] C. Chen, Y. Wu, R. Li, The development of new NLO crystals in the borate series, J. Cryst. Growth 99 (1990) 790–798.
- [32] B.F. Levine, Bond-charge calculation of nonlinear optical susceptibilities for various crystal structures, Phys. Rev. B 7 (1973) 2600–2626.
- [33] C. Chen, Z. Lin, Z. Wang, The development of new borate-based UV nonlinear optical crystals, Appl. Phys. B 80 (2005) 1–25.
- [34] W. Yao, R. He, X. Wang, Z. Lin, C. Chen, Analysis of deep-UV nonlinear optical borates: approaching the end, Adv. Opt. Mater. 2 (2014) 411–417.
- [35] R. Xiao, H. Wu, Y. Ni, Z. Wang, C. Huang, M. Qi, C. Ge, A modified method to simulate the dispersion properties of infrared nonlinear optical crystals, J. Appl. Phys. 117 (2015) 135702.
- [36] Optical properties in CASTEP, CASTEP Documentation, University of Cambridge, https://www.tcm.phy.cam.ac.uk/castep/documentation/WebHelp/content/ modules/castep/thcastepopticalprops.htm.
- [37] Q. Sun, W. Yang, Y. Cheng, J. Dong, M. Zhu, B. Zhang, A. Dubois, M. Zhu, W. Jie, Y. Xu, Anisotropic dielectric behavior of layered perovskite-like Cs3Bi2I9 crystals in the terahertz region, Phys. Chem. Chem. Phys. 22 (2020) 24555–24560.
- [38] C. Parlak, R. Eryiğit, Ab initio volume-dependent elastic and lattice dynamical properties of chalcopyrite \$\mathrm{Cu}\mathrm{Ga}{\mathrm{Se}}_{2}, Phys. Rev. B 73 (2006) 245217.
- [39] Y. Cai, L. Zhang, Q. Zeng, L. Cheng, Y. Xu, First-principles study of vibrational and dielectric properties of β–Si3N4, Phys. Rev. B 74 (2006).
- [40] K. Karch, T. Dietrich, W. Windl, P. Pavone, A.P. Mayer, D. Strauch, Contribution of quantum and thermal fluctuations to the elastic moduli and dielectric constants of covalent semiconductors, Phys. Rev. B 53 (1996) 7259–7266.

- [41] L. Hu, D. Wei, X. Huang, Second harmonic generation property of monolayer TMDCs and its potential application in producing terahertz radiation, J. Chem. Phys. 147 (2017) 244701.
- [42] S.J. Clark, M.D. Segall, C.J. Pickard, P.J. Hasnip, M.I.J. Probert, K. Refson, M. C. Payne, First principles methods using CASTEP, Z. Kristallogr. Cryst. Mater. 220 (2005) 567–570.
- [43] D. Zagorac, H. Müller, S. Ruehl, J. Zagorac, S. Rehme, Recent Developments in the Inorganic Crystal Structure Database: Theoretical Crystal Structure Data and Related Features.
- [44] J.P. Perdew, K. Burke, M. Ernzerhof, Generalized gradient approximation made simple, Phys. Rev. Lett. 77 (1996) 3865.
- [45] G. Kresse, J. Furthmüller, Efficient iterative schemes for ab initio total-energy calculations using a plane-wave basis set, Phys. Rev. B 54 (1996) 11169.
- [46] D.R. Hamann, M. Schlüter, C. Chiang, Norm-conserving pseudopotentials, Phys. Rev. Lett. 43 (1979) 1494.
- [47] V. Lucarini, J.J. Saarinen, K.-E. Peiponen, E.M. Vartiainen. Kramers-Kronig relations in optical materials research, Springer Science & Business Media, 2005.
- [48] I. Petousis, W. Chen, G. Hautier, T. Graf, T.D. Schladt, K.A. Persson, F.B. Prinz, Benchmarking density functional perturbation theory to enable high-throughput screening of materials for dielectric constant and refractive index, Phys. Rev. B 93 (2016) 115151
- [49] H.J. Monkhorst, J.D. Pack, Special points for Brillouin-zone integrations, Phys. Rev. B 13 (1976) 5188.
- [50] J.P. Perdew, A. Zunger, Self-interaction correction to density-functional approximations for many-electron systems, Phys. Rev. B 23 (1981) 5048–5079.
- [51] Z. Li, Z. Lin, Y. Wu, P. Fu, Z. Wang, C. Chen, Crystal growth, optical properties measurement, and theoretical calculation of BPO4, Chem. Mater. 16 (2004) 2906–2908
- [52] Basic Nonlinear Optical Crystals, in: D.N. Nikogosyan (Ed.), Nonlinear Optical Crystals: A Complete Survey, Springer, New York, NY, 2005, pp. 5–74.
- [53] Newly Developed and Perspective Crystals, in: D.N. Nikogosyan (Ed.), Nonlinear Optical Crystals: A Complete Survey, Springer, New York, NY, 2005, pp. 215–275.